Korean J. Chem. Eng., 36(11), 1915-1921 (2019)
DOI: 10.1007/s11814-019-0377-9

pISSN: 0256-1115
eISSN: 1975-7220

Preparation of magnetic activated carbon-chitosan nanocomposite for crystal violet adsorption

Ferda Civan Çavuşoğlu, Seher Akan, Ezgi Aleyna Arı, Ezgi Çetinkaya, Elif Çolak, Gamze Nur Daştan, Semina Deniz, Damla Erdem, Melda Köksal, Sevgi Korkmaz, Nursena Onsekiz, Betül Oruçoğlu, Didem Özkaya, Hamdi Buğra Uslu, Çağlanur Ünal, Oğulcan Yıldız, Şeyma Özkara-Aydınoğlu, and Şahika Sena Bayazit†

Beykent University, Engineering & Architecture Faculty, Chemical Engineering Department, 34396 Istanbul, Turkey
(*Received 22 May 2019 • accepted 28 August 2019*)

Abstract−Magnetic, cheap and versatile adsorbents were developed for crystal violet (CV) adsorption in this study. These adsorbents are magnetic activated carbon (AC-Fe_3O_4) and chitosan grafted magnetic activated carbon (Chitosan-AC-Fe_3O_4). Fe_3O_4 and chitosan were also used for adsorption. X-ray diffraction (XRD), scanning electron microscopy (SEM), vibrating sample magnetometer (VSM), zeta potential analysis and Fourier transform infrared spectroscopy (FTIR) methods were used for characterization of adsorbents. Adsorption parameters for CV were investigated. Raw chitosan and Fe_3O_4 were also used for CV adsorption to compare the results of composites. The chosen adsorption parameters are amount of adsorbent, contact time, initial CV concentration, and temperature. The equilibrium period was observed to be very short for chitosan and Fe_3O_4 nanoparticles. The adsorption efficiencies of these adsorbents are very low. AC-Fe_3O_4 and AC-Fe_3O_4-Chitosan nanoparticles reached equilibrium at 80 min. The all adsorbent-CV systems followed pseudo second-order kinetic model. AC-Fe_3O_4 and AC-Fe_3O_4-Chitosan composites suited non-linear Freundlich isotherm for all temperatures (298, 308 and 318 K). Regeneration of adsorbents was also investigated. 1 M of acetic acid and 0.1 M of NaOH solutions were tested. Acetic acid solution desorbed CV better than NaOH solution at 6 hours.

Keywords: Crystal Violet, Adsorption, Activated Carbon, Magnetite, Chitosan

INTRODUCTION

In recent years, water pollution has become a major problem worldwide, with industrial waste one of the most important reasons for water pollution [1]. Dye pollution is generally created by textile, leather, paper and cosmetics industries [2,3]. It is estimated that more than 10,000 different dyes are used worldwide annually [4]. Dyes are complex compounds containing multicolored, toxic and carcinogenic substances; thus dyes pose serious threats to humans and aquatic organisms [5,6].

Crystal violet (CV) is a widely known dye that is often used as a colorant in paper, leather and textiles industries [1,4]. It is known that even 1 ppb crystal violet is toxic to humans and animals. It is important to treat industrial waste from CV before it is discharged for environmental safety [1,7].

To remove dyes from wastewater, several methods have been used. Adsorption, ion exchange, membrane filtration, chemical and physical precipitation, supercritical oxidation processes, ozonation, distillation, photocatalysis and other approaches are some examples for wastewater treatment [3,5,6]. Among these methods, adsorption is more advantageous because of its simple operation, relatively low cost, flexibility, recyclability, efficiency of the process and no sludge production [3,6,7].

The removal efficiency of dyes depends on surface properties of the chosen adsorbents [7]. Various adsorbents, such as activated carbon, zeolite, silica and natural-based (shells, fruit peels) biopolymers, have been studied and applied [8]. Activated carbon is an efficient adsorbent for dye adsorption because of high adsorption capacity and wide surface area. In addition, it is possible to modify the chemical and physical properties of activated carbon by various methods [2,9].

Besides, activated carbons which have adsorbed pollutants also cause a second pollution in the treatment processes. The use of magnetic activated carbon is an attractive option to overcome this problem as separation of magnetic materials is simpler and more efficient [1].

In recent years, the magnetic characteristics of nanomaterials have found increasing applications, such as in magnetic separation [6]. Some magnetic metal oxide powders (such as Fe_2O_3, Fe_3O_4, and Al_2O_3) are known as potential adsorbents [7]. Fe_3O_4 nanoparticles have been widely used due to their simple synthesis, relatively low cost, and less environmental impact. By now, highly efficient and environmentally friendly based surface-modified magnetic nano adsorbents have been used to remove metal ions and organic dyes [6].

Recently, it has been possible to remove the dyes by using adsorption method with chitosan, differently from conventional wastewater treatment methods [2]. Chitosan is a promising material for biopolymer-based adsorbents, as it is non-toxic, biodegradable and environmentally friendly [3,5].

Chitosan, a kind of copolymer, consists of 2-glucosamine and N-acetyl-2glucosamine [2]. The chitosan structure contains amine and hydroxyl functional groups. Therefore, the sulfonyl, carboxyl,

†To whom correspondence should be addressed.
E-mail: sahikasena@gmail.com

acetyl and alkyl groups available in the dye structure can easily interact with the functional groups of the chitosan structure [10].

Several researchers have studied dye adsorption using different adsorbents. Monash and Pughazhenti used MCM-41 for CV adsorption [11]. Li et al. prepared modified biochar for Orange II adsorption [12]. Graphene is also used for dye adsorption as a carbon compound. Kazeem et al. prepared graphene/double hydroxide composites and adsorbed anionic dyes from water [13]. Metal oxides are also used for removal of dyes, Hossienzadeh et al. prepared ZnO for this purpose [14].

In this work, crystal violet adsorption was performed using synthesized magnetic adsorbent. Magnetic activated carbon-chitosan was synthesized by a coprecipitation technique. Four different adsorbents were used in the crystal violet adsorption process: chitosan, Fe_3O_4, magnetic activated carbon and magnetic activated carbon-chitosan nanocomposite. Using these adsorbents, the influence of initial dye concentration, adsorbent amount, retention time and adsorption temperature was investigated. Consequently, Langmuir and Freundlich isotherms and kinetics of adsorption process were studied.

MATERIALS AND METHOD

Chitosan and crystal violet ($C_{25}H_{30}N_3Cl$) were purchased from Sigma-Aldrich Co., activated carbon (AC), HNO_3, acetic acid, NaCl, ethanol, HCl, NaOH, NH_3 (25%) solution, $FeSO_4{\cdot}7H_2O$ and $Fe(NO_3)_3{\cdot}9H_2O$ salts were obtained from Merck Co.

1. Method

Chitosan, Fe_3O_4, AC-Fe_3O_4 and AC-Fe_3O_4-Chitosan composites were used for CV adsorption. Chitosan was used as received.

1-1. Preparation of Fe_3O_4 Nanoparticles

Co-precipitation method was used for preparation of Fe_3O_4 nanoparticles. According to the method, Fe(II) and Fe(III) salts were dissolved in water under ultrasonication. The molar ratio of the mixture was Fe(II) : Fe(III)=1 : 2. After preparing the mixture, 8 M NH_3 solution was added dropwise, till pH of the mixture reached 11-12. Obtained Fe_3O_4 nanoparticles were washed with water and ethanol, then dried under vacuum at 50 °C [15].

1-2. Preparation of AC-Fe_3O_4 Composite

First, raw activated carbon was contacted with concentrated HNO_3 under ultrasonication for 100 min. Then, oxidized activated carbon was washed with water until pH value of AC reaches 7. Drying process was carried out under vacuum at 50 °C. AC-Fe_3O_4 composite prepared using co-precipitation method is explained below [15].

1-3. Preparation of AC-Fe_3O_4-Chitosan Composite

Co-precipitation method was used for preparation of AC-Fe_3O_4-Chitosan composites. 0.1% (w/v) chitosan solution was added to Fe(II), Fe(III) and AC mixture. Then precipitation, washing and drying processes were applied accordingly [15,16].

1-4. Characterization Methods

X-ray diffraction (XRD), Fourier transform infrared spectroscopy (FTIR) and scanning electron microscopy (SEM) methods were applied to composites. Bruker axis D8 was used for XRD analysis (Cu Kα radiation λ=1.540 Å). Bruker Alpha spectrometer was used for recording FTIR spectra. The range of wavenumber was from 400 to 4,000 cm^{-1}. KBr method was used for analysis. The morphology of composites was determined by Quanta FEG 250 Field emission scanning electron microscope (FESEM), FEI Company. The magnetic properties were measured at room temperature by vibrating sample magnetometer (VSM) up to a magnetic field of ±5 kOe. Zeta potential analysis was performed using a Malvern Zetameter (Malvern Instruments).

Adsorption studies were carried out at batch type using an incubator shaker. Some process variables were investigated for determining the optimum adsorption conditions and maximum CV adsorption uptake of composites. Also, bare Fe_3O_4 and chitosan particles were investigated for CV adsorption. The adsorption parameters are amount of adsorbent, initial CV concentration, temperature and time. The range of adsorbent quantity was 100 mg/L-1 g/L. The initial CV concentrations were 2-25 mg/L. The selected temperatures were 298, 308, 318 K. The period of shaking was 0-120 min. First, the optimum amount of adsorbent was determined. 100, 250, 500, 750 and 1,000 mg/L of adsorbents were weighed and 10 mL of 15 mg/L of CV solution was added to them. These mixtures were shaken for 120 min (due to pre-experiments). Second, equilibration times were determined for all adsorbents. Optimum amount of adsorbent was chosen and 10 mL of 15 mg/L of CV solution was added to them. These kinetic data also were used for kinetic modelling calculations. Non-linear pseudo-first-order, pseudo-second-order models, Weber-Morris intraparticle diffusion model and Elovich model were chosen for this study. Finally, the effect of initial CV concentration was determined. The chosen concentrations were 2-25 mg/L. Optimum adsorbent quantity and equilibration time was used for all adsorbents. The obtained data were also used for calculation of equilibrium isotherm. Non-linear Langmuir and Freundlich isotherms were used for this study.

Desorption experiments were carried out batch mode. 0.1 M of NaOH and 1 M acetic acid solution was applied for CV desorption. Acetic acid was chosen as desorption eluent after pre-experiments. The optimum CV adsorption conditions were used for desorption studies. After adsorption, adsorbents were removed from solutions by magne, and were washed with water, dried at room temperature. Then, desorption eluent was added to adsorbents and shaken for 6 hours. The second and third adsorption processes were applied to these adsorbents.

RESULTS AND DISCUSSION

1. Characterization Results

The prepared adsorbents are Fe_3O_4, AC-Fe_3O_4 and AC-Fe_3O_4-Chitosan nanoparticles. Chitosan was used as received for comparison. SEM, XRD, FTIR, zeta potential and VSM methods were applied to determine the structure of adsorbents.

Fig. 1 shows the SEM images of AC, AC-Fe_3O_4-Chitosan and chitosan. As seen in Fig. 1(a), oxidized activated carbon (AC) has amorphous morphology and chitosan has polymeric morphology (Fig. 1(c)). In Fig. 1(b), AC-Fe_3O_4 nanocomposites gathered together through chitosan.

XRD patterns of AC, Fe_3O_4, AC-Fe_3O_4 are seen in Fig. 2(a). The characteristic peaks of Fe_3O_4 nanoparticles are displayed in patterns of AC-Fe_3O_4 nanoparticles. The addition of chitosan causes noise in

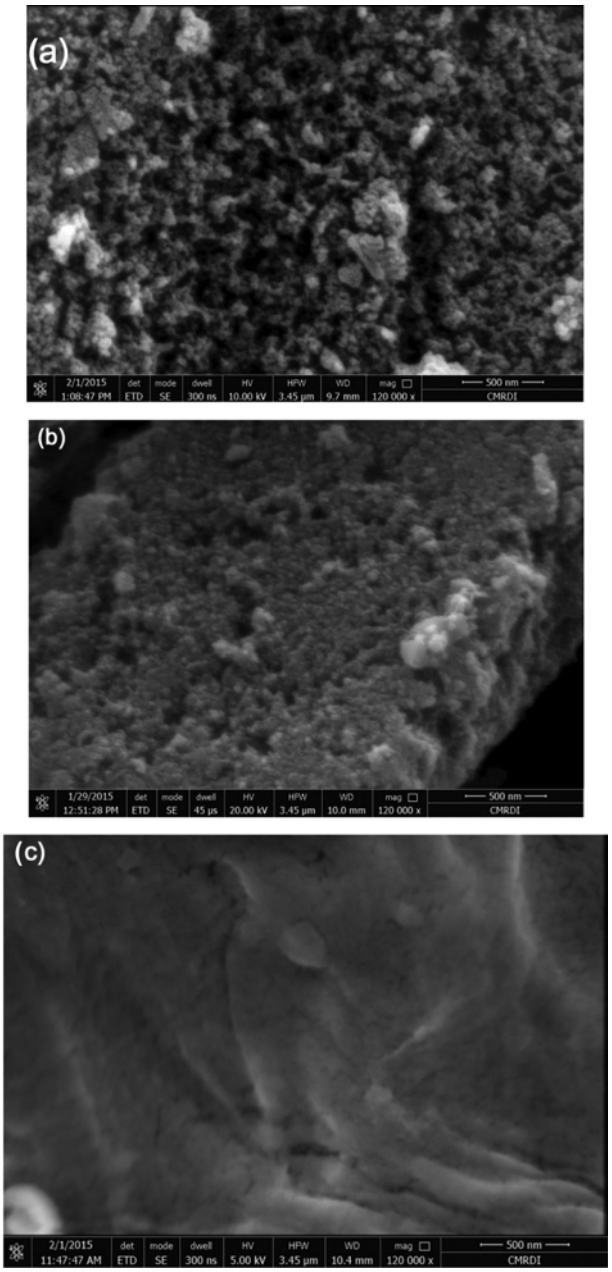

Fig. 1. SEM images of oxidized AC (a), AC-Fe_3O_4-Chitosan (b), Chitosan (c).

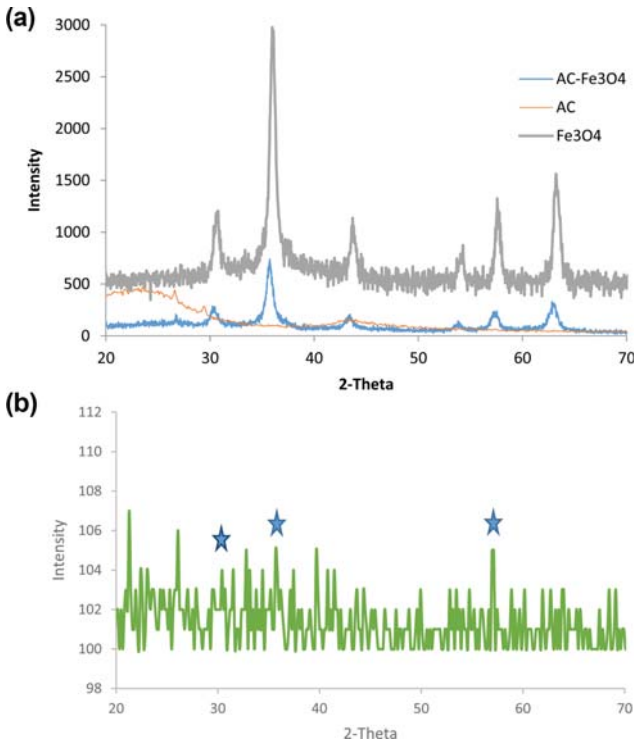

Fig. 2. XRD patterns of (a) AC, AC-Fe_3O_4 and Fe_3O_4; (b) Chitosan-ACFe_3O_4.

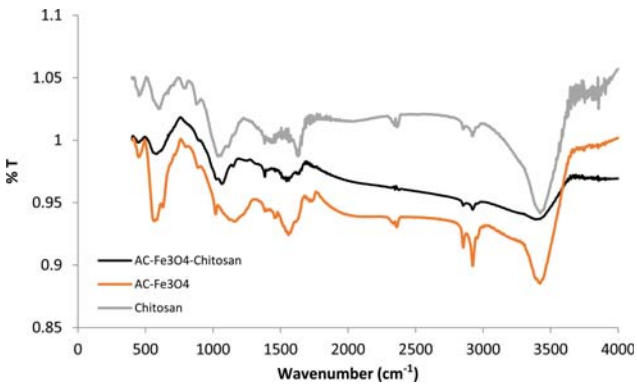

Fig. 3. FTIR plots of AC-Fe_3O_4-Chitosan, AC-Fe_3O_4 and Chitosan.

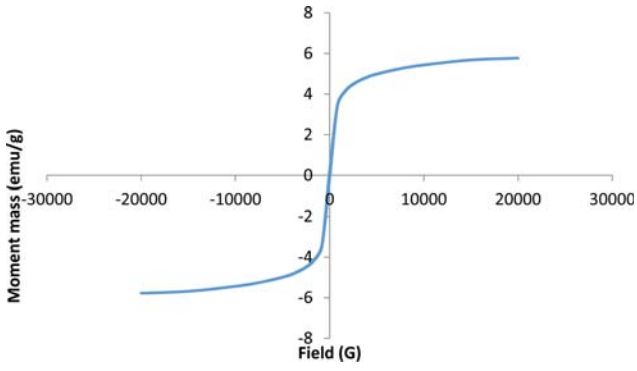

Fig. 4. VSM plot of AC-Fe_3O_4-Chitosan.

AC-Fe_3O_4-Chitosan composites as seen in Fig. 2(b). Some Fe_3O_4 peaks can be seen at 30.7°, 35.68° and 57.28°. So, the pattern was not given in Fig. 2. The characteristic peaks of Fe_3O_4 are 30.7°, 35.68°, 43.3°, 54.4°, 57.2° and 63.04° [16].

FTIR plots of AC-Fe_3O_4-Chitosan, AC-Fe_3O_4 and Chitosan are presented in Fig. 3. In AC-Fe_3O_4 plot, strong Fe-O vibration (593 cm^{-1}) of Fe_3O_4 can be seen. Chitosan addition reduces the intensity of Fe-O vibration peak [17]. The C-O stretching band of chitosan at 1,072 cm^{-1} appears at AC-Fe_3O_4-Chitosan, but there is not this peak in AC-Fe_3O_4. The intensity of C-H stretching peak at 2,926 cm^{-1} decreases with addition of chitosan. The intensities of O-H stretching peak of Chitosan and AC-Fe_3O_4 at 3,450 cm^{-1} de-

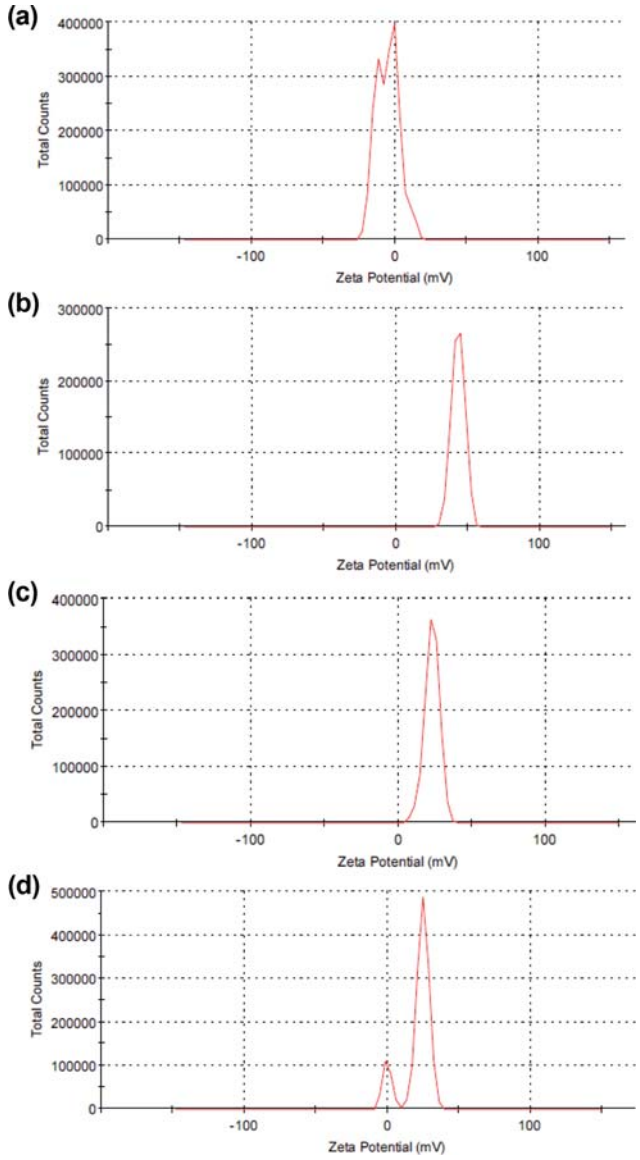

Fig. 5. Zeta potential plots of AC-Fe_3O_4 (a), Chitosan-AC-Fe_3O_4 (b), Fe_3O_4 (c), Chitosan (d).

crease while combining both of them.

Magnetic properties of AC-Fe_3O_4-Chitosan were determined by vibrating sample magnetometer. The curve is given in Fig. 4. Generally, Fe_3O_4 nanoparticles have high magnetization values. For example, Hu et al. obtained this value as 73.5 emu·g^{-1} [18]. The addition of AC and chitosan causes decreasing of the magnetization. As shown in Fig. 4, the magnetization value was obtained as 5.78 emu·g^{-1}.

Zeta potential analysis plots of all adsorbents are given in Fig. 5. Water was used as dispersant. Zeta potential value of AC-Fe_3O_4 is −5.12 mV, AC-Fe_3O_4-Chitosan is 43.1 mV, Fe_3O_4 is 22.7 mV, and chitosan is 20.9 mV. Zeta potential values that are between ±10 mV and ±30 mV, the colloidal stabilities of adsorbents are incipient. The colloidal stabilities of AC-Fe_3O_4, Fe_3O_4 and chitosan are incipient. Zeta potential values that are between ±30 mV and ±40 mV, the stabilities of the adsorbents are moderate [19]. The stability of AC-Fe_3O_4-Chitosan is better than the other adsorbents.

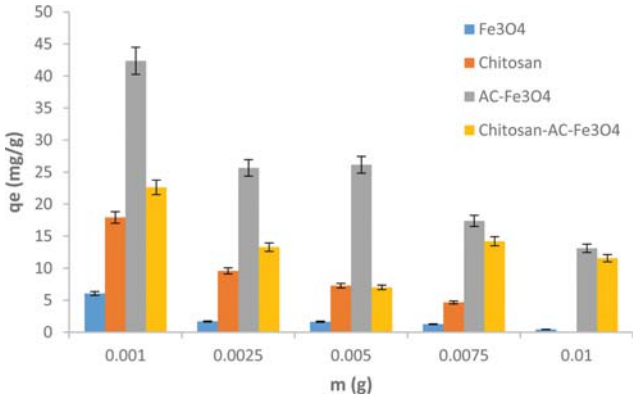

Fig. 6. The effect of amount of adsorbent on CV adsorption.

2. Adsorption Studies

The result of the effect of adsorbent quantity is given in Fig. 6. The range of adsorbent quantity was 1 mg-10 mg. Adsorption loading (q_e) values at equilibrium were calculated using Eq. (1) as follows:

$$q_e = \frac{(C_0 - C_e) \times V}{m} \quad (1)$$

C_0 and C_e are initial and equilibrium CV concentrations as mg·L^{-1}. V is volume of the adsorption solution as L; m is the adsorbent quantity as g. Fe_3O_4, chitosan, AC-Fe_3O_4 and AC-Fe_3O_4-Chitosan were used for determining the adsorption efficiencies of composites. The q_e values of Fe_3O_4 differ between 6.05 mg/g-0.44 mg/g, while the amount of Fe_3O_4 differs between 1 mg-10 mg. Similarly, adsorption loading values of chitosan are 17.92-4.66 mg/g. At 10 mg of adsorbent quantity, a significant result cannot be obtained. AC-Fe_3O_4 has the highest adsorption efficiency. AC-Fe_3O_4-Chitosan also has quite high adsorption capacity. The adsorption capacity of AC-Fe_3O_4 is 42.37 mg/g at 1 mg. The other experiments were carried out at 1 mg.

The equilibrium time of the adsorbent-CV systems was determined at room temperature. The experimental data were used for calculating pseudo-first-order model and pseudo-second-order kinetic models. The equations of these models are given below.

$$q_t = q_e(1 - e^{-k_1 t}) \quad (2)$$

$$q_t = \frac{t_2 q_e^2 t}{1 + k_2 q_e t} \quad (3)$$

Eq. (2) is non-linear pseudo-first-order kinetic model [20], q_t is adsorption loading at t time, k_1 (min^{-1}) is rate constant. Eq. (3) is non-linear second-order kinetic model [21]. k_2 is rate constant for a kinetic model of pseudo-second-order (g·mg^{-1}·min^{-1}). Non-linear pseudo-first-order kinetic model plots of Fe_3O_4, chitosan, AC-Fe_3O_4 and AC-Fe_3O_4-Chitosan can be seen in Fig. 7. Non-linear pseudo-second-order kinetic model plots are represented in Fig. 8, and the model parameters are given in Table 1. As shown in Fig. 7-8, Fe_3O_4 and chitosan have very low adsorption capacities, so equilibrium periods of these adsorbents are very short. The composites reach equilibrium state in approximately 80 minutes. All adsorbents follow pseudo-second-order kinetic model. The reaction mechanisms between adsorbent and adsorbate depend on chemisorption

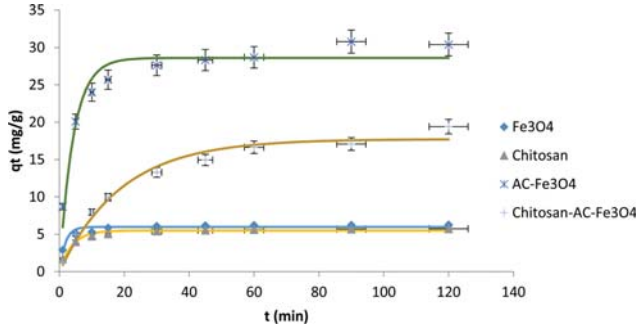

Fig. 7. Non-linear pseudo-first order kinetic model plots of CV adsorption.

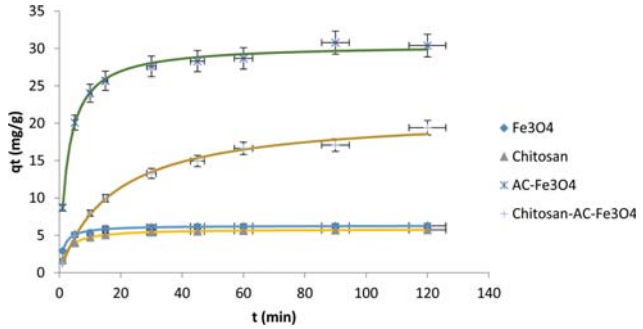

Fig. 8. Non-linear pseudo-second order kinetic model plots of CV adsorption.

involving valency forces through the sharing or exchange of electrons as covalent forces, and ion exchange. The reaction rates are increasing when composites are used as adsorbents. The k_2 values of AC-Fe_3O_4 and AC-Fe_3O_4-Chitosan are 0.012 and 0.003 g·mg^{-1}·min^{-1}, respectively. Weber-Morris intraparticle diffusion (IPD) model was applied to experimental data. The IPD model equation is given in Eq. (4):

$$q_t = k_d t^{1/2} + c \tag{4}$$

q_t (mg/g) is adsorption uptake at t time. k_d (mg/g min$^{1/2}$) is rate constant. IPD model plots are given in Fig. 9. The IPD plots formed

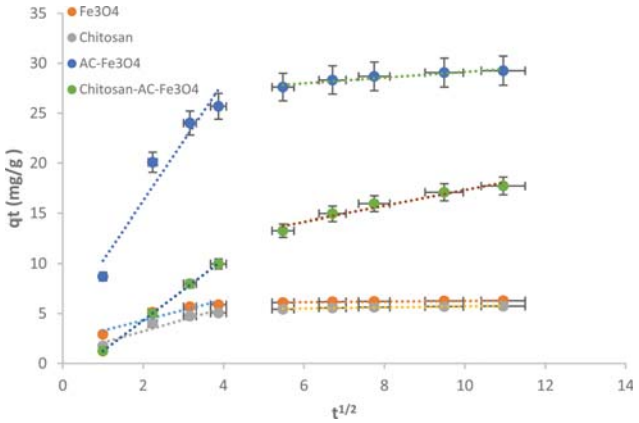

Fig. 9. Weber-Morris intraparticle diffusion model plots.

two straight lines. This means adsorption system occurs in two stages. The first stage is the boundary layer diffusion and the second stage is the intraparticle diffusion step [22]. According to k_d values, it seems that the boundary layer diffusion step is faster than intraparticle diffusion step for all adsorbents. Elovich model is one of the most applied kinetic models for chemisorption [23]. The Elovich equation is given in Eq. (5):

$$q_t = \frac{1}{\beta}\ln(\alpha\beta) + \left(\frac{1}{\beta}\right)\ln(t) \tag{5}$$

In Eq. (5), α is initial adsorption rate (mg/gmin), β (mg/g) is adsorption constant that is related to the extent of surface coverage and activation energy [24]. α and β values are given in Table 1. The Elovich plots are given in Fig. 10. The correlation coefficients of the model are between 0.83-0.98. According to correlation coefficients of kinetic models, it is understood that the pseudo-second-order kinetic model adapts to all adsorbents.

Langmuir [25] and Freundlich [26] isotherms were calculated for determining the adsorption mechanisms and equlibrium conditions of the systems:

$$q_e = \frac{K_L q_m C_e}{1 + K_L C_e} \tag{6}$$

Table 1. Kinetic model parameters of CV adsorption

	Pseudo-first-order kinetic model			Pseudo-second-order kinetic model		
	q_e (mg/g)	k_1 (min^{-1})	Adj. R^2	q_e (mg/g)	k_2	Adj. R^2
Fe_3O_4	5.98	0.578	0.87	6.31	0.132	0.98
Chitosan	5.50	0.261	0.95	5.85	0.074	0.99
AC-Fe_3O_4	28.59	0.234	0.93	30.54	0.012	0.99
AC-Fe_3O_4-Chitosan	17.73	0.053	0.97	21.21	0.003	0.99
	IPD			Elovich model		
	k_{d1}	R^2	k_{d2}	R^2	α	β	R^2
Fe_3O_4	1.03	0.88	0.03	0.92	6.72	1.57	0.83
Chitosan	1.15	0.93	0.05	0.92	17.60	1.27	0.89
AC-Fe_3O_4	5.95	0.93	0.28	0.92	81.53	0.24	0.89
AC-Fe_3O_4-Chitosan	3.06	0.99	0.78	0.95	3.92	0.27	0.98

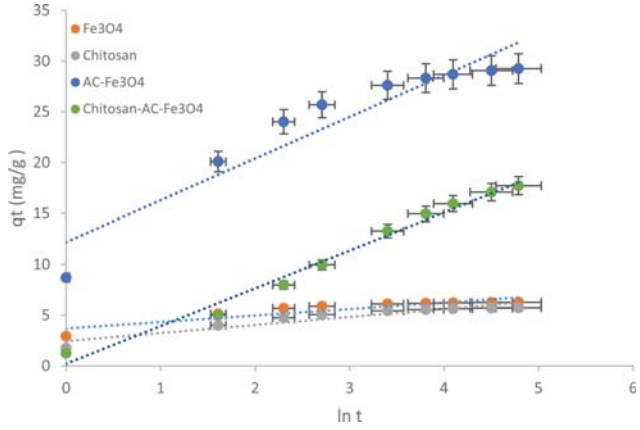

Fig. 10. Elovich kinetic model plots.

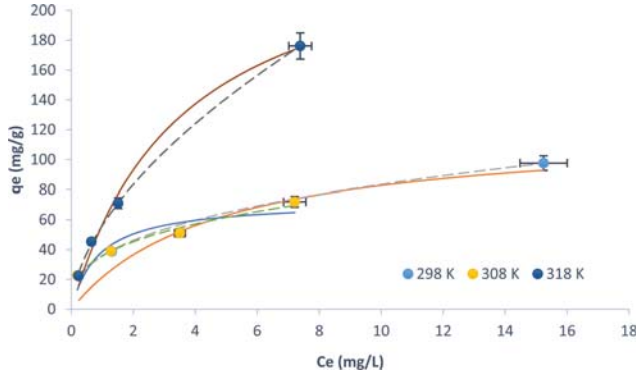

Fig. 11. Non-linear Langmuir and Freundlich isotherm plots of AC-Fe_3O_4, symbols represent experimental results, straight lines represent Langmuir isotherm plots and dotted lines represent Freundlich isotherm plots.

$$q_e = K_f C_e^{1/n} \quad (7)$$

The equilibrium isotherm models were applied to experimental data. The nonlinear Langmuir (Eq. (6)) and Freundlich isotherm (Eq. (7)) plots of AC-Fe_3O_4 and AC-Fe_3O_4-Chitosan can be seen in Figs. 11 and 12, respectively. In Eq. (6), K_L (mg/L) is Langmuir constant and q_m (mg/g) is maximum adsorption uptake. In Eq. (7), K_f and 1/n are Freundlich model constants, indicating capacity and intensity of adsorption, respectively [27]. Three different temperatures were chosen for isotherm experiments: 298, 308 and 318 K.

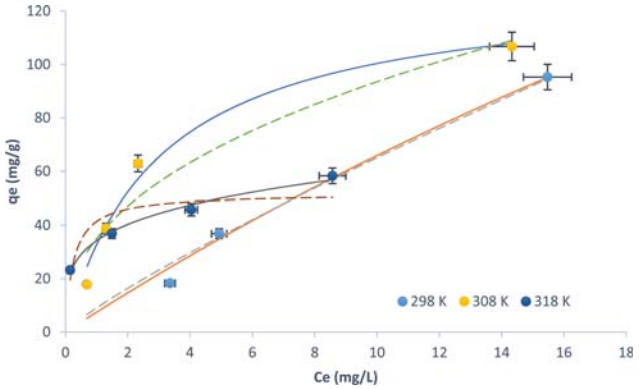

Fig. 12. Non-linear Langmuir and Freundlich isotherm plots of AC-Fe_3O_4-Chitosan, symbols represent experimental results, straight lines represent Langmuir isotherm plots and dotted lines represent Freundlich isotherm plots.

The isotherm parameters are shown in Table 2. Significant isotherm parameters for Fe_3O_4 and chitosan were not obtained, so these results were not represented in this study. According to correlation coefficients, the adsorption processes for both of the adsorbents were following Freundlich isotherm for all temperatures. The Freundlich isotherm generally represents heterogeneous adsorption systems. The 1/n values can express the adsorption mechanism. For example; if 1/n<1, the adsorption mechanism depends on chemisorption [28]. As seen in Table 2, the mechanisms of adsorption systems for both of the adsorbents are chemisorption. And if 1/n values are closer to zero, the heterogeneity of the system increases. The heterogeneity of AC-Fe_3O_4-Chitosan increases while temperature increases. According to Langmuir parameters, q_m values of AC-Fe_3O_4 at 318 K and AC-Fe_3O_4-Chitosan at 298 K can be compared to literature. Because, adjusted R^2 values of AC-Fe_3O_4 and AC-Fe_3O_4-Chitosan are 0.89, 0.97, respectively. CV adsorption capacity of AC-Fe_3O_4 is 266.57 mg/g, AC-Fe_3O_4-Chitosan is 505.87 mg/g. Chakraborty et al. prepared NaOH modified rice husk and reached adsorption capacity of 39.96 mg/g at 313 K, 44.87 mg/g at 293 K [29]. Tahir et al. prepared chitosan aniline, chitosan pyrrole and starch for CV adsorption. The obtained qm values are 54.91, 150.16 and 10.25 mg/g, respectively [30].

Desorption experiments were carried out at batch mode. 0.1 M of NaOH and 1 M acetic acid solutions was tried for CV desorption. It was determined at pre-experiments that acetic acid solution is more suitable for AC-Fe_3O_4 and AC-Fe_3O_4-Chitosan. De-

Table 2. Isotherm parameters of CV adsorption

		Langmuir isotherm				Freundlich isotherm			
		q_m (mg/g)	K_L	Adj. R^2	Red. Chi-sqr	K_f	1/n	Adj R^2	Red. Chi-sqr
AC-Fe_3O_4	298	120.93	0.22	0.69	324.28	35.82	0.37	0.99	1.35
	308	72.75	1.13	0.75	105.37	36.02	0.33	0.97	11.34
	318	266.57	0.21	0.89	57.33	56.18	0.57	0.99	2.50
AC-Fe_3O_4-Chitosan	298	505.87	0.015	0.92	101.15	9.08	0.85	0.93	91.92
	308	130.22	0.34	0.97	41.28	35.07	0.43	0.89	157.94
	318	51.74	4.02	0.67	70.65	34.24	0.24	0.98	3.74

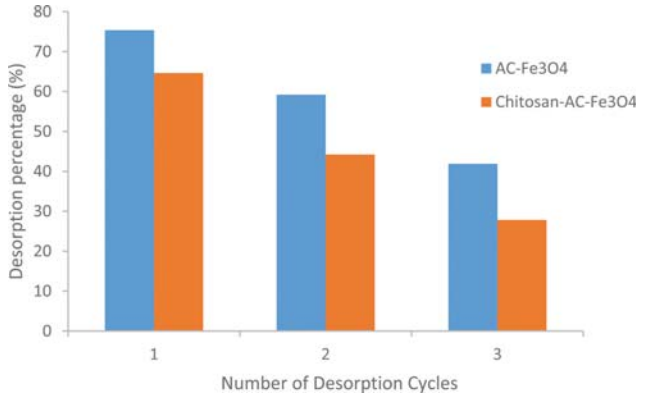

Fig. 13. Desorption cycle plots of AC-Fe_3O_4 and Chitosan-AC-Fe_3O_4.

sorption calculations were made by Eq. (8):

$$\text{des}\,(\%) = \frac{\text{Desorbed CV}}{\text{Adsorbed CV}} \times 100 \tag{8}$$

Desorption plots are given in Fig. 13. According to pre-experiments, equilibration time of desorption was determined as six hours. Desorption experiments were carried out as three cycles. 75.35% of CV was desorbed from AC-Fe_3O_4 at first cycle and 41.87% of CV was desorbed at third cycle. 64.63% of CV was desorbed from AC-Fe_3O_4-Chitosan at first cycle and 27.84% of CV desorbed at third cycle.

CONCLUSION

Fe_3O_4, AC-Fe_3O_4 and AC-Fe_3O_4-Chitosan nanoparticles were prepared using co-precipitation method and characterized by FTIR, XRD, SEM, zeta potential and VSM. Chitosan was also used for CV adsorption. The parameters of CV adsorption were investigated. The adsorbent quantity was determined as 1 mg for all adsorbents. The equilibrium period was very short for chitosan and Fe_3O_4 nanoparticles. The adsorption efficiency of these adsorbents is very low. AC-Fe_3O_4 and AC-Fe_3O_4-Chitosan nanoparticles reached equilibrium at 80 min. The reaction kinetics of adsorption followed the pseudo-second-order kinetic model. The experimental data were fitted to nonlinear Freundlich isotherm at all temperatures for both AC-Fe_3O_4 and AC-Fe_3O_4-Chitosan nanoparticles. The maximum theoretical adsorption capacity was 266.57 mg/g at 318 K for AC-Fe_3O_4 nanoparticles; 505.87 mg/g at 298 K for AC-Fe_3O_4-Chitosan nanoparticles. The adsorbents used in this study are environmentally friendly. The preparation method of these composites is easy and cheap. CV adsorption capacities of AC-Fe_3O_4 and AC-Fe_3O_4-Chitosan nanoparticles are more effective according to literature. And magnetic properties provide easy separation and reuse of adsorbents. Regeneration studies of AC-Fe_3O_4 and AC-Fe_3O_4-Chitosan were carried out as three cycles. Desorption rates for AC-Fe_3O_4 75.35% at first cycle and 41.87% at third cycle. Desorption rates for AC-Fe_3O_4-Chitosan 64.63% at first cycle and 27.84% at third cycle.

REFERENCES

1. P. Rai, R. K. Gautam, S. Banerjee, V. Rawat and M. C. C. Chattopadhyaya, *J. Environ. Chem. Eng.*, **3**(4), 2281 (2015).
2. H. Jayasantha Kumari, P. Krishnamoorthy, T. K. K. Arumugam, S. Radhakrishnan and D. Vasudevan, *Int. J. Biol. Macromol.*, **96**, 324 (2017).
3. B. Xu, H. Zheng, Y. Wang, Y. An, K. Luo, C. Zhao and W. Xiang, *Int. J. Biol. Macromol.*, **112**, 648 (2018).
4. L. Sellaoui, G. L. Dotto, E. C. Peres, Y. Benguerba, É. C. Lima, A. Ben Lamine and A. Erto, *J. Mol. Liq.*, **248**, 890 (2017).
5. M. Hui, P. Shengyan, H. Yaqi, Z. Rongxin, Z. Anatoly and C. Wei, *Chem. Eng. J.*, **345**(March), 556 (2018).
6. Y. Huo, H. Wu, Z. Wang, F. Wang, Y. Liu, Y. Feng and Y. Zhao, *Colloids Surf., A Physicochem. Eng. Asp.*, **549**(February), 174 (2018).
7. R. Fabryanty, C. Valencia, F. E. Soetaredjo, J. N. Putro, S. P. Santoso, A. Kurniawan, Y.-H. H. Ju and S. Ismadji, *J. Environ. Chem. Eng.*, **5**(6), 5677 (2017).
8. N. H. Othman, N. H. Alias, M. Z. Shahruddin, N. F. Abu Bakar, N. R. Nik Him and W. J. Lau, *J. Environ. Chem. Eng.*, **6**(2), 2803 (2018).
9. T. N. V. de Souza, S. M. L. de Carvalho, M. G. A. Vieira, M. G. C. da Silva and D. do S. B. Brasil, *Appl. Surf. Sci.*, **448**, 662 (2018).
10. S. E. Subramani and N. Thinakaran, *Process Saf. Environ. Prot.*, **106**, 1 (2017).
11. P. Monash and G. Pugazhenthi, *Adsorption*, **15**(4), 390 (2009).
12. G. Li, H. Li, X. Mi and W. Zhao, *Korean J. Chem. Eng.*, **36**(8), 1274 (2019).
13. T. S. Kazeem, M. Zubair, M. Daud, N. D. Mu'azu and M. A. Al-Harthi, *Korean J. Chem. Eng.*, **36**(7), 1057 (2019).
14. K. Hossienzadeh, A. Maleki, H. Daraei, M. Safari, R. Pawar and S. M. Lee, *Korean J. Chem. Eng.*, **36**(8), 1360 (2019).
15. S. Qu, J. Wang, J. Kong, P. Yang and G. Chen, *Talanta*, **71**(3), 1096 (2007).
16. S. T. Danalıoğlu, Ş. S. Bayazit, Ö. Kerkez Kuyumcu and M. A. Salam, *J. Mol. Liq.*, **240**, 589 (2017).
17. A. K. Bordbar, A. A. Rastegari, R. Amiri, E. Ranjbakhsh, M. Abbasi and A. R. Khosropour, *Biotechnol. Res. Int.*, **2014**, 705068 (2014).
18. P. Hu, L. Kang, T. Chang, F. Yang, H. Wang, Y. Zhang, J. Yang, K. Wang, J. Du and Z. Yang, *J. Alloys Compd.*, **728**, 88 (2017).
19. M. S. A. Darwish and I. Stibor, *J. Dispers. Sci. Technol.*, **37**, 1793 (2016).
20. S. Lagergren and K. Sven. *Vetenskademiens Handl.*, **24**, 1 (1898).
21. Y. S. Ho and G. McKay, *Process Biochem.*, **34**(5), 451 (1999).
22. J. Wan, T. Tao, Y. Zhang, X. Liang, A. Zhou, C. Zhu, J.-W. Choi and S. Luo, *RSC Adv.*, **6**(28), 23233 (2016).
23. H. I. Inyang, A. Onwawoma and S. Bae, *Soil Tillage Res.*, **155**, 124 (2016).
24. L. Largitte and R. Pasquier, *Chem. Eng. Res. Des.*, **109**, 495 (2016).
25. I. Langmuir, *J. Am. Chem. Soc.*, **40**(9), 1361 (1918).
26. H. Freundlich, *Zeitschrift F{ü}r Phys. Chemie*, **57**, 385 (1906).
27. H. Wei, L. Han, Y. Tang, J. Ren, Z. Zhao and L. Jia, *J. Mater. Chem. B*, **3**(8), 1646 (2015).
28. K. Y. Foo and B. H. Hameed, *Chem. Eng. J.*, **156**(1), 2 (2010).
29. S. Chakraborty, S. Chowdhury and P. Das Saha, *Carbohydr. Polym.*, **86**(4), 1533 (2011).
30. N. Tahir, H. N. Bhatti, M. Iqbal and S. Noreen, *Int. J. Biol. Macromol.*, **94**, 210 (2017).